# **JAAS**



# **PAPER**

View Article Online
View Journal | View Issue



**Cite this:** *J. Anal. At. Spectrom.*, 2024, **39**, 439

# analysis by secondary ionization mass spectrometry†

A corundum reference material for oxygen isotope

Sebastian Schmidt, \*\*D\*\*\* Andreas Hertwig, \*\*D\*\*\* Axel Karl Schmitt, \*

A synthetic laser ruby crystal (HD-LR1) is introduced as a new matrix-matched reference material for secondary ionization mass spectrometry (SIMS) analysis of oxygen isotopes in corundum. Laser fluorination isotope ratio mass spectrometry (LF-IRMS) bulk analyses of multiple mg-sized fragments are homogenous, averaging  $\delta^{18}O = +18.40 \pm 0.14\%$  (95% confidence interval, n=23) and  $\Delta'^{17}O = -0.368 \pm 0.005\%$  (as deviation from slope 0.528 for  $\delta'^{17}O$  vs.  $\delta'^{18}O$  at 95% conf., n=11) relative to Vienna Standard Mean Ocean Water (V-SMOW). SIMS spot analyses show homogeneous O-isotopic values at the ng-scale independent of the location in the HD-LR1 single crystal and in four different crystallographic orientations. However, sample surface topography as an artefact of polishing corundum embedded in epoxy creates excess variability in  $\delta^{18}O$  within  $\sim$ 100  $\mu$ m from the edges of the grains. HD-LR1 is a chemical pure crystal with only Cr as a trace component detected at 276  $\mu$ g g<sup>-1</sup> by EPMA, whereas Be, often introduced in artificial gem enhancement, is <0.002  $\mu$ g g<sup>-1</sup> based on SIMS analyses. Therefore, HD-LR1 can also be used as a reference material for Cr, or as a blank for other trace element analyses of corundum by SIMS or LA-ICP-MS.

Received 10th July 2023 Accepted 27th November 2023

DOI: 10.1039/d3ja00229b

rsc.li/jaas

# Introduction

Corundum (Al<sub>2</sub>O<sub>3</sub>) is a mineral of significant scientific and economic interest. It is present in meteorites as one of the oldest solids in the solar system, and a key indicator mineral in high-grade metasediments. Moreover, corundum is prized as a gemstone (Fig. 1A) in its two varieties, sapphire and ruby, which show vibrant colours resulting from minor and trace chemical impurities. Corundum and its gem varieties are primary in igneous and metamorphic settings, which are complemented by secondary occurrences, either as volcanic xenocrysts typically associated with alkaline basalts, or in placer deposits due to its physical and chemical stability.

As a major component in corundum, oxygen and its isotopes (<sup>16</sup>O, <sup>17</sup>O, and <sup>18</sup>O) can provide valuable information on how

corundum formed in extra-terrestrial and terrestrial geological environments. Mass-dependent and mass-independent fractionation leads to variations in isotopic abundance (expressed as δ<sup>18</sup>O in relation to Vienna Standard Mean Ocean Water V-SMOW) and potential deviations from the mass-dependent fractionation line (expressed as  $\Delta'^{17}$ O relative to a slope of 0.528 in the three-isotope ratio diagram). Although trace elements in corundum can be used to classify corundum according to formation environment and geographic origin,5 the rather pure chemical composition of corundum and the significant overlap in trace element abundances (particularly in the case of blue sapphire) from different geographic localities<sup>6,7</sup> limit their discriminatory power. Oxygen isotopes in corundum, by contrast, are highly variable depending on the formation environment and type (sapphire vs. ruby)8 and thus can help to enable traceability of gems in global supply chains.6 Moreover, synthetic corundum can often be distinguished from natural ones by negative anomalies in  $\Delta'^{17}O$  inherited from tropospheric oxygen.9

The interpretation of the oxygen isotopic compositions in corundum is significantly enhanced when deciphered at high spatial resolution. The precise determination of oxygen isotopic compositions ( $\delta^{18}$ O,  $\Delta'^{17}$ O) at the microscale is the domain of secondary ionization mass spectrometry (SIMS) using large-geometry ion microprobes. This enables interpretation of data within a petrologic context and the detection of intracrystalline

<sup>&</sup>quot;Institut für Geowissenschaften, Universität Heidelberg, Im Neuenheimer Feld 236, 69120 Heidelberg, Germany. E-mail: sebastian.schmidt@alumni.uni-heidelberg.de bJohn de Laeter Centre, Curtin University, Bentley, WA 6102, Australia 'Earth, Planetary, and Space Sciences, University of California Los Angeles, 595 Charles Young Drive East, Los Angeles, CA 90095-1567, USA

<sup>&</sup>lt;sup>4</sup>Department of Earth Sciences, University of Oregon, Eugene, OR 97403, USA <sup>\*</sup>Geowissenschaftliches Zentrum, Georg-August-Universität, Goldschmidtstraße 1, 37073 Göttingen, Germany

<sup>†</sup> Electronic supplementary information (ESI) available: Table of SIMS oxygen isotope analyses of corundum and NIST SRM 610 reference glass. See DOI: https://doi.org/10.1039/d3ja00229b

JAAS Paper

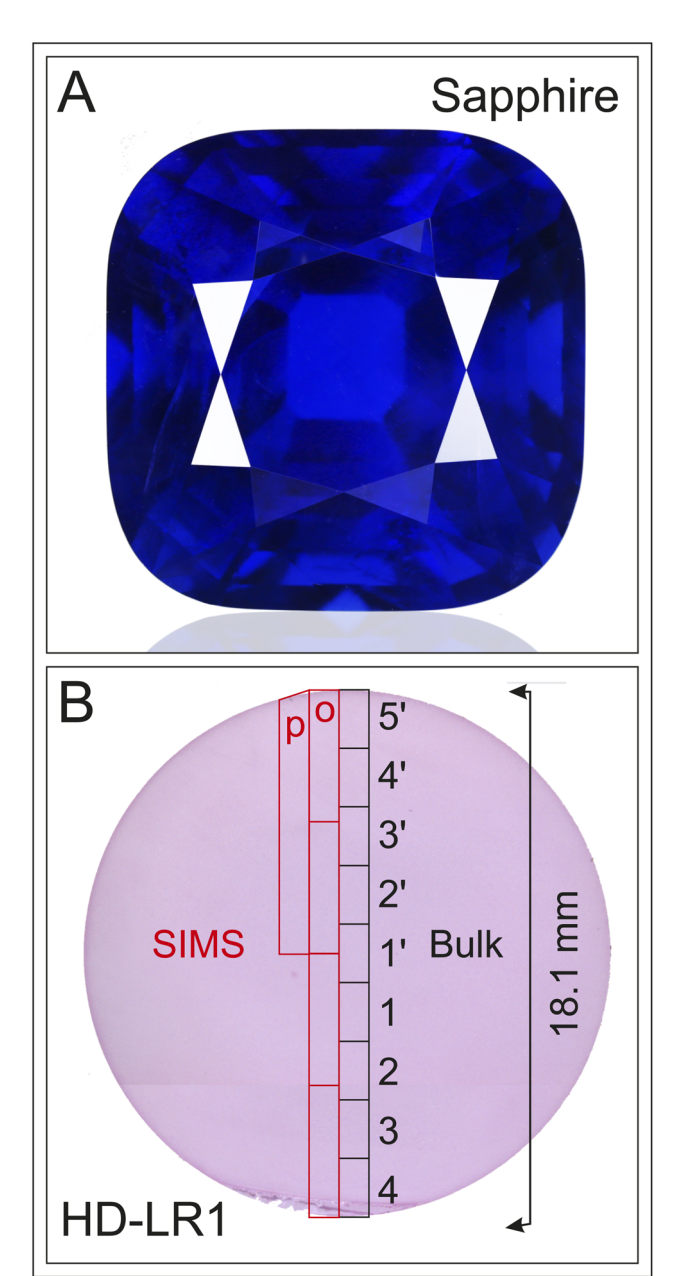


Fig. 1 Photographs of (A) a gem-quality untreated blue Burmese sapphire, weight: 56 carats (=11.2 g), dimensions:  $20 \times 20 \times 14$  mm (photo courtesy Gübelin Gem Lab) and (B) 1.5 mm thick disk of HD-LR1 with saw cuts indicated for LF-IRMS and SIMS analyses. Numbers correspond to Table 2, whereas letters "p" and "o" indicate slices used for SIMS profile and crystal orientation analysis (after re-orientation), respectively. Although slice "p" is  $\sim 9$  mm long, only the inner 6 mm were exposed after embedding in epoxy.

zonation. The minimally destructive nature of SIMS even allows for analysing valuable cut gemstones. $^{10}$ 

An essential requirement for accurate SIMS analysis is the availability of matrix-matched reference materials.<sup>11</sup> Although natural and synthetic corundum references have been used by different SIMS labs,<sup>2,12,13</sup> these are of limited availability and often lack a detailed compositional characterization. Moreover, crystal orientation can potentially create instrumental bias

effects in SIMS oxygen isotope analysis that have not been systematically evaluated for corundum. Because corundum is isostructural with hematite (space group  $R\bar{3}c$ ),<sup>14</sup> and crystal orientation effects have been previously reported for oxygen isotope analysis of hematite by ion microprobe (SHRIMP-SI),<sup>15</sup> it appears prudent to quantify the extent of these effects also for corundum.

Here, we report results for the characterization of a synthetic laser ruby (HD-LR1) as a matrix-matched reference material for SIMS oxygen isotope analysis of corundum using chemical, isotopic, and structural analysis (Fig. 1B) considering the ISO Guide 35.<sup>16</sup> Purity of HD-LR1 was assessed by energy dispersive spectrometry (EDS) and trace abundances for common natural (Mg, Ti, V, Cr, Fe, and Ga) and potential synthetic impurities (Be) were quantified by electron microprobe analysis (EPMA) and SIMS, respectively. Bulk oxygen isotope analyses were carried out at the mg-scale by laser fluorination isotope ratio mass spectrometry (LF-IRMS), and *in situ* analyses at the ng-scale by SIMS using differently oriented crystals as verified by electron backscatter diffraction (EBSD).

# Experimental

#### Laser ruby (HD-LR1): description and preparation

HD-LR1 is a synthetic crystal that was originally part of a laser at the Lawrence Livermore National Laboratory from where it was obtained by one of us (KDM). Termed ruby in material science, these crystals were typically synthesized by the Czochralskimethod whereby a cylindrical boule of corundum with the growth axis at  $60^{\circ}$  to the c axis is slowly extracted from molten  $Al_2O_3$  doped with small quantities of Cr.<sup>17</sup> The crystal orientation (verified by EBSD) confirms this for HD-LR1. The 18.1 mm diameter rod was cut into several 1.5 mm thick disks (Fig. 1B); two of these  $\sim$ 1.6 g disks were retained at the department of Earth, Planetary, and Space Sciences at UCLA, and the other two were used and partly consumed in this study at Heidelberg University.

One entire disk was first embedded in epoxy resin within a 25.4 mm inner diameter Teflon mould, and multiple  $\sim$ 1 mm wide bars were sliced from the epoxy round using a low-speed saw with a diamond blade. Subsequently the bars were removed from the epoxy resin that was softened by heating on a hotplate to  $\sim$ 150 °C. Millimetre-sized fragments for LF-IRMS analysis were obtained across one slice by sawing and crushing in a steel mortar and pestle. An adjacent slice was sectioned in four pieces, which were mounted in different crystal orientations within a 25.4 mm epoxy round. NIST SRM 610 glass fragments were added around the pieces of HD-LR1. Another slice was mounted in the centre of another 25.4 mm diameter epoxy mount for microanalysis homogeneity tests. Evaluating different sample preparation steps, a procedure was developed that produced flat surfaces (within 2-3 µm relief) by grinding with 220, 600, and 1200 grit diamond on a grinding wheel (MD-Piano, Struers), and polishing surfaces with a 3 µm diamondsuspension (DP-Suspension P, Struers) and an alcohol-based lubricating agent (DP-Lubricant Blue, Struers) on a rubber-like surface polishing wheel (MD-Largo, Struers). This was

repeated using 2 µm and 1 µm diamond-suspension and folsequential ultrasonic cleaning enediaminetetraacetic acid + ammonia, purified water, and methanol. For EPMA and SIMS analyses a conductive coating (carbon 9 nm or gold 50 nm, respectively) was applied, with a gentle re-polishing to remove the coating and cleaning of the surfaces between them. Sample topography was measured using a Bruker DektakXT stylus profilometer in mapping mode at Heidelberg University.

#### Compositional analysis

Electron microprobe (EPMA). The chemical composition of HD-LR1 was determined using a JEOL SuperProbe JXA-iSP100 equipped with five wavelength dispersive spectroscopy (WDS) detectors at Heidelberg University operated at 15 kV acceleration voltage, 100 nA beam current (focused beam), and 11 mm working distance. Natural and synthetic mineral standards were used for calibration of Mg, Ti, V, Cr, Fe, and Ga. Peak count times of 300 s were applied except for Cr (200 s) and Fe (100 s); background counts were integrated for half these durations. Limits of detection at 95% confidence level under these conditions based on instrument software were: 10 µg g<sup>-1</sup> (Mg),  $22 \mu g g^{-1}$  (Ti),  $16 \mu g g^{-1}$  (V),  $32 \mu g g^{-1}$  (Cr),  $48 \mu g g^{-1}$  (Fe), and 36 $\mu g g^{-1}$  (Ga).

Beryllium abundances by SIMS. Beryllium abundance in HD-LR1 was quantified by SIMS using a CAMECA IMS 1280 HR at Heidelberg University. A primary beam of <sup>16</sup>O<sup>-</sup> ions at 23 keV and with  $\sim$ 1 nA intensity was focussed to a spot size of  $\sim$ 10  $\mu m$ in diameter. Secondary ions of 9Be+ and 27Al3+ were accelerated to 10 keV and detected at a mass resolving power (MRP) of  $\sim$ 1600 in the axial electron multiplier (EM) by electrostatic peak switching using a deflector located after the magnet (DSP2x) while maintaining a steady magnetic field via a high-precision nuclear magnetic resonance (NMR) probe. Counts were integrated over five cycles totalling 50 and 20 s, respectively. A relative sensitivity factor was calibrated by measuring the multidoped synthetic corundum reference material 02-1267-21 (ref. 5) with 2.58  $\mu g$  g<sup>-1</sup> Be. Limits of detection based on EM background count rate were  $\sim 0.002 \ \mu g \ g^{-1}$ .

Crystal orientation (EBSD). To obtain designated crystallographic orientations of HD-LR1 for SIMS analysis, we first confirmed that the laser ruby was oriented with the c axis at  $60^{\circ}$ relative to the long axis of the original rod. Subsequently, pieces were cut using a diamond saw and secured with Kapton adhesive tape on carefully prepared epoxy wedges that allowed the pieces to be cast in epoxy in the desired orientation. Through cutting with a diamond saw and grinding as described above, surfaces were exposed, and a total of four oriented pieces were placed along with NIST SRM 610 glass in a single epoxy mount. To check for misorientations that might have been introduced through sample preparation, EBSD point analyses were performed on a JEOL JSM-IT800 field emission gun scanning electron microscope (FEG-SEM) with an Oxford Instruments Symmetry2 detector at Heidelberg University. The high vacuum mode was used with 18 kV accelerating voltage and 8 nA beam current. Sample tilt was 70° with a working distance of 23 mm.

The EBSD data were processed in the AZtecCrystal software (Version 2.2, Oxford Instruments).

#### Oxygen isotopic analysis

Laser fluorination isotope ratio mass spectrometry. Oxygen isotope analyses of HD-LR1 fragments were carried out in LF-IRMS labs at University of Oregon (UO) and University of Göttingen (GÖ) using dual inlet systems of MAT253 and Finnigan Delta plus mass spectrometers, respectively. Values for  $\delta^{18}$ O use V-SMOW  $^{18}\text{O}/^{16}\text{O} = 0.0020052,^{18}$  and  $\Delta'^{17}\text{O}$  values are reported relative to the reference line with slope 0.528 and zero intercept in the  $\delta'^{17}$ O vs.  $\delta'^{18}$ O space.

Sessions at UO included fluorination of 16 HD-LR1 single fragments with a mass of 0.6-1.5 mg and analysis of gas using both  $O_2$  (n = 2) or  $CO_2$  (n = 14) methods. Analyses were normalized using in-house UOG garnet ( $\delta^{18}O = +6.52\%$ ), 19 UWG2 ( $\delta^{18}O = +5.80\%$ ), 20 San Carlos Olivine (SCO,  $\delta^{18}O =$ +5.25%,  $\Delta'^{17}O = -0.051\%$ ) and high- $\delta^{18}O$  standard Stevens Klint Flint (SKFS,  $\delta^{18}O = +33.93\%$ ,  $\Delta'^{17}O = -0.114\%$ ). Repeatability for these silicate reference materials is  $\pm 0.1\%$  for  $\delta^{18}$ O and  $\pm 0.01\%$  for  $\Delta'^{17}$ O; the observed larger scatter for HD-LR1 relative to the silicate values is accounted for by stating an overall error based on the standard deviation of corundum analyses. A scale compression correction of 0.5%/18 = 0.038%was applied to match data obtained by CO<sub>2</sub> and O<sub>2</sub> methods of light and heavy references and unknowns.

Nine aliquots of HD-LR1 with masses ranging from 1.4-2.2 mg were analysed at GÖ. Following laser fluorination and gas purification, samples were measured relative to a reference gas calibrated using O2 released from SCO.9 On the basis of replicate analyses of SCO, the analytical uncertainty in  $\delta^{18}$ O and  $\Delta'^{17}$ O are assumed to be  $\pm 0.2\%$  and  $\pm 0.01\%$ , respectively. Further details on the analytical procedure are summarized in ref. 22.

Secondary ionization mass spectrometry. SIMS analysis of oxygen isotopes in HD-LR1 were carried out to (1) assess homogeneity of  $\delta^{18}$ O and  $\Delta'^{17}$ O at the ng-sampling scale, and (2) evaluate a potential instrumental bias caused by crystal orientation. This involved multiple analytical sessions on a CAMECA IMS 1280 HR ion microprobe at Heidelberg University in multicollection mode. A primary beam of Cs<sup>+</sup> at 23 keV impact energy and with an  $\sim$ 1-2 nA focussed beam was rastered over a 10  $\times$  10 μm<sup>2</sup> area, and a normal-incidence electron gun was tuned to overlap the rastered area for optimal charge compensation. The mass spectrometer was tuned to resolve molecular ion interferences (16OH and H216O on 18O and 17O, requiring MRP of  $\sim$ 2000 and  $\sim$ 6000, respectively). Either <sup>16</sup>O and <sup>18</sup>O (L2' and H1 Faraday Cup FC detectors), or <sup>16</sup>O, <sup>17</sup>O, and <sup>18</sup>O (L2', FC2, and H1 FCs) were simultaneously detected with a  $10^{10} \Omega$  resistor for measuring  $^{16}O$  and  $10^{12}$   $\Omega$  resistors for the minor isotopes. A static magnetic field was maintained by NMR regulation, and integration times were adjusted to achieve <0.2\% (2 standard error; SE) internal precision for the relevant isotopic ratios. Prior to acquisition, the surface was pre-sputtered for 20-30 s and deflectors in the transfer section automatically centred. After each analysis, the 16OH signal was monitored and a 16OH-

**JAAS** Paper

tail correction applied to the  $\delta^{17}O$  values (0.04-0.07% for natural corundum and HD-LR1). Raw intensities were adjusted for detector yields in relation to two in-line reference voltages, and FC baselines were subtracted using a running average of measured counts integrated over the 20-30 s pre-sputtering with the secondary ion beam deflected. Analytical reproducibility for δ<sup>18</sup>O over different domains of the mount surface was monitored by replicate analysis of NIST SRM 610 glass surrounding HD-LR1. External reproducibility of NIST SRM 610 was between 0.24 and 0.42% (2SD) on the HD-LR1 crystal orientation mount where targets covered a comparatively large area (up to  $\sim$ 6 mm from the centre); the overall reproducibility (without any correction for primary beam intensity drift) on NIST SRM 610 was 0.47% (2SD, n = 22) suggesting negligible *X*-Y effects. All analyses for the same session were normalized to the bulk value determined by LF-IRMS. IMF values in different sessions were between 0.995 and 0.997, and the resulting sputter craters reached a depth of  $\sim$ 0.26 µm as determined by Bruker DektakXT stylus profilometer, corresponding to a sample mass of  $\sim 0.25$  ng per analysis spot for the nominal density of corundum (4 g cm<sup>-3</sup>).

In a separate setup, a stronger  $\sim$ 5 nA primary beam was used for determining the  $\Delta'^{17}O$  of HD-LR1. For this, a calibration curve in  $\delta'^{17}$ O vs.  $\delta'^{18}$ O was established using natural terrestrial corundum of variable isotopic composition assuming that these have  $\Delta'^{17}O = -0.052 \binom{9}{90}$  relative to the reference line with slope 0.528 and zero intercept in the  $\delta'^{17}$ O vs.  $\delta'^{18}$ O space. For all SIMS analyses of this study, the internal precision (2SE) is considered to represent the analytical uncertainty of individual analyses.

### Results & discussion

#### Chemical composition of HD-LR1

A total of 174 individual EPMA analyses of HD-LR1 were collected, for which only Cr was detectable above background at an abundance of 276  $\pm$  29  $\mu g$  g<sup>-1</sup> (2SD). In all EPMA analyses the levels of Mg, Ti, V, Fe, and Ga were below the limits of detection (Table 1). Similarly, Be spot analyses by SIMS (n = 12) are <0.002  $\mu g g^{-1}$  and Be thus are negligible in HD-LR1 (Table 1). This is consistent with the synthetic origin of HD-LR1, where only Cr is present as a minor dopant.

#### Oxygen isotopic composition

HD-LR1  $\delta^{18}$ O values of LF-IRMS analyses for fragments of 9 cut out slices across the disk (Fig. 1) average +18.40  $\pm$  0.14% (95%) confidence interval calculated from the standard error of the mean multiplied with the student t-value considering the appropriate degree of freedom; n = 23; Fig. 2A and Table 2A). For  $\Delta'^{17}$ O, HD-LR1 deviates significantly from the reference line of natural corundum with an average of  $-0.368 \pm 0.005\%$  (95%)

Table 1 Summary of compositional data for HD-LR1

	Mg	Ti	V	Cr	Fe	Ga	Ве
$\mu g g^{-1}$	<10	<22	<16	$276\pm29$	<48	<36	< 0.002

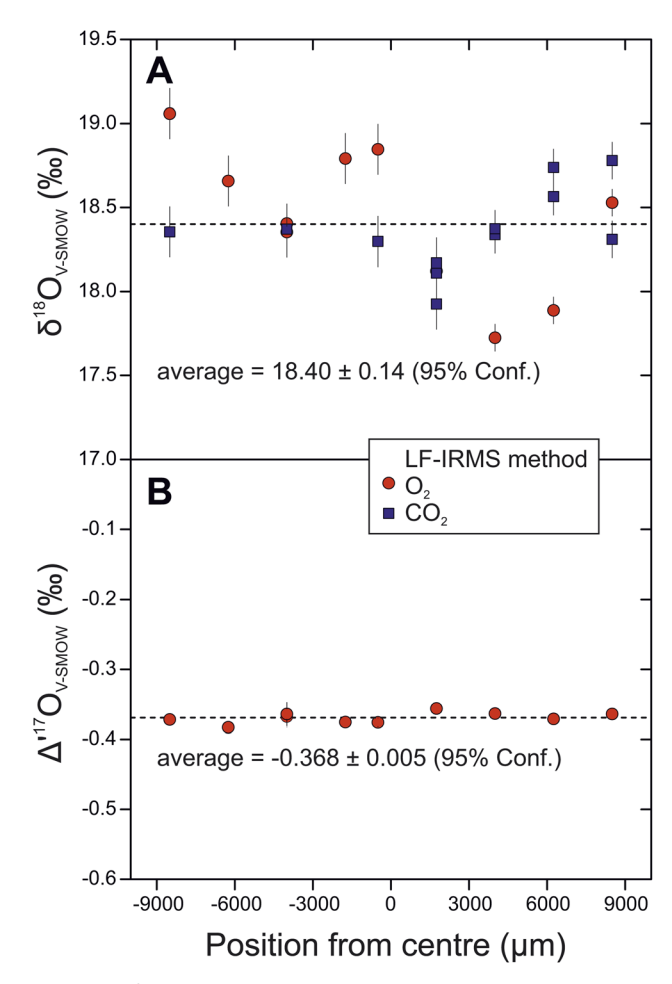


Fig. 2 (A)  $\delta^{18}$ O and (B)  $\Delta'^{17}$ O individual values and averages determined by LF-IRMS relative to position of fragments analysed in HD-LR1 disk. Error bars are based on repeatability of silicate references; for HD-LR1, 2 SE = standard error were calculated from  $2\times$  standard deviation divided by the square-root of replicates.

conf.; n = 11; Fig. 2B). Data for the edge of the rod vs. the centre are indistinguishable based on one-way ANOVA test results for  $\delta^{18}$ O (see ESI†). In this test, position from the centre of the disk is the factor under consideration and the mean of results from UO and GÖ LF-IRMS laboratories were treated as replicates. With a p-value of 0.52, no significant effect due to the factor was observed, i.e.,  $\delta^{18}$ O values are independent from the position of sampling.

A SIMS profile ( $\delta^{18}$ O) on a  $\sim$ 6 mm long slice from the centre to the edge of a HD-LR1 disk was analysed in quadruplicate in  $\sim$ 100 µm and  $\sim$ 300 µm steps in x- and y-directions, respectively. The reproducibility of 76 spots equals 0.27% (2SD) (Fig. 3A) and is identical to that obtained on homogeneous glass. The exception are spots that were placed within  $\sim$ 100  $\mu$ m of the edge due to topography, as discussed on the next section (Fig. 4). One-way ANOVA testing suggests a significant (p = 0.04) influence of the factor (the position from the centre) on the  $\delta^{18}$ O data. However, this is only due to one set of four replicates with high repeatability at position  $-5689 \mu m$  (18.20  $\pm$  0.07% 1SD; Fig. 3A). This may represent a true (but minor) isotopic heterogeneity or outlier data where the statistical effect is

Table 2 Summary of oxygen isotope data by LF-IRMS against position in disk for HD-I R1

Position from							
centre (µm)	Lab code	Method	δ <sup>18</sup> O (‰)	Δ′ <sup>17</sup> O (‰)			
8500	UO 1-4	$CO_2$	18.78				
8500	UO 1-4	$CO_2$	18.31				
8500	GÖ 2-4	$O_2$	18.53	-0.364			
6250	UO 1-3	$CO_2$	18.56				
6250	UO 1-3	$CO_2$	18.74				
6250	GÖ 2-3	$O_2$	17.89	-0.371			
4000	UO 1-2	$CO_2$	18.34				
4000	UO 1-2	$CO_2$	18.37				
4000	GÖ 2-2	$O_2$	17.72	-0.363			
1750	UO 2-1	$CO_2$	18.11				
1750	UO 2-1	$CO_2$	18.17				
1750	UO 1-1	$CO_2$	17.93				
1750	GÖ 2-1	$O_2$	18.12	-0.356			
-500	UO 1-1'	$CO_2$	18.30				
-500	GÖ 1-1′	$O_2$	18.85	-0.376			
-1750	GÖ 1-2′	$O_2$	18.79	-0.375			
-4000	UO 2-3'	$CO_2$	18.37				
-4000	UO 3-3'	$O_2$	18.40	-0.364			
-4000	GÖ 1-3′	$O_2$	18.35	-0.368			
-6250	GÖ 1-4′	$O_2$	18.66	-0.383			
-8500	UO $2-5'$	$CO_2$	18.35				
-8500	GÖ 1-5′	$O_2$	19.06	-0.372			
Random	UO 3-r	$O_2$	18.48	-0.354			
Average			18.40	-0.368			
SD			0.33	0.009			
95% conf.			0.14	0.005			
N			23	11			

amplified by their high repeatability. When excluding this single set, testing shows that  $\delta^{18}$ O values are independent of the position within the slice (p = 0.24) and, hence, a homogeneous oxygen isotopic composition at the scale of  $\sim$ 300  $\mu m$  steps is inferred.  $\Delta^{\prime 17}$ O values were determined in replicate (n = 5-6) on the same slice, representing central, intermediate, and rim locations of the HD-LR1 disk. The values are indistinguishable within uncertainty for each location and yielded an average  $\Delta'^{17}O = -0.39 \pm 0.05\%$  (95% conf., n = 17; Fig. 3B). One-way ANOVA testing underlines that position within the slice does not significantly affect  $\Delta'^{17}$ O values (p = 0.24). A  $\Delta'^{17}$ O value of -0.39 is significantly different from 0 and agrees within uncertainty with the more precise LF-IRMS measurements albeit with much smaller sample consumption. In addition to these systematic tests on a centre-edge slice through the HD-LR1 disk, random fragments of HD-LR-1 were analysed in replicate (n = 172) in two additional analytical sessions and on six different mounts. In these cases, the repeatability was on average 0.45% (2SD) for  $\delta^{18}$ O, further attesting to the smallscale homogeneity of HD-LR1. This also holds for  $\Delta'^{17}$ O values from 91 analyses on random fragments of HD-LR1 on three different mounts with an average repeatability of 0.30% (2 SD).

#### Crystal orientation and topography effects

HD-LR1 in four different orientations was analysed in a single session on the same mount along with NIST SRM 610 glass as a monitor for X-Y effects and instrumental drift. The four

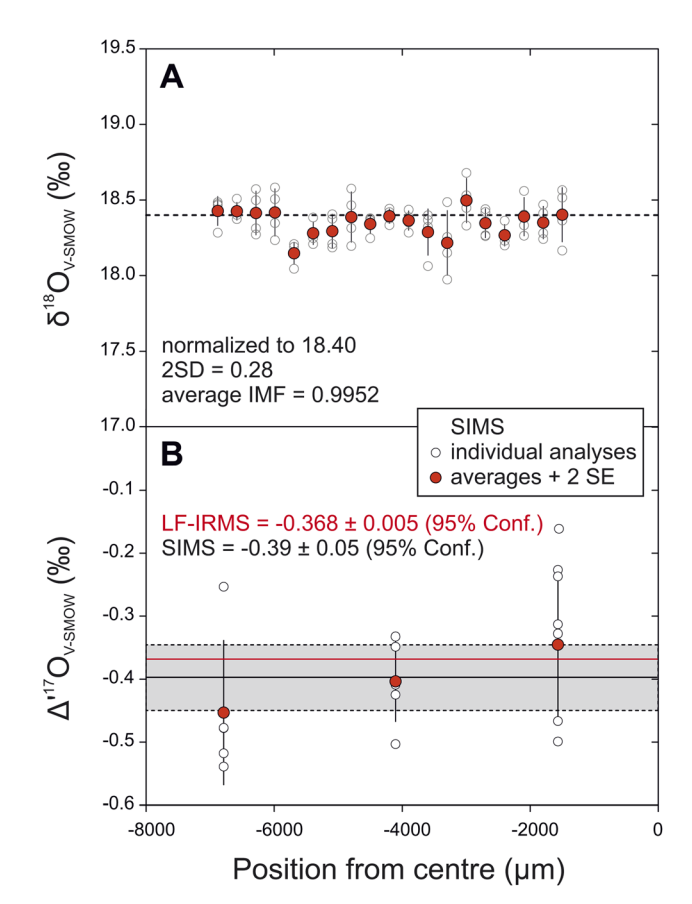


Fig. 3 Individual and averaged  $\delta^{18}$ O (A) and  $\Delta'^{17}$ O (B) values determined by SIMS relative to the position on a 6 mm slice of HD-LR1. Values for  $\delta^{18}$ O are normalized to the LF-IRMS average with the resulting IMF stated; LF-IRMS average for  $\Delta'^{17}$ O is plotted as red horizontal line. 2 SE standard errors plotted as in Fig. 2.

orientations (Fig. 5) account for (1) the likely orientation of natural corundum when crystals are laid down on adhesive tape on well-developed crystal faces (i.e. {0001} or {1120} designated as  $\perp c$  and  $\parallel c$ , respectively), and (2) density of atomic packing relative to the primary ion beam; these are named c60 and c60'.15

The incident angle between the secondary ion optical axis (the z-direction in CAMECA instruments) and the primary ion optical axis (nominally 30°) is modified by the secondary ion extraction field acting on the primary ion beam. For the conditions used (primary accelerating potential -13 kV; secondary accelerating potential +10 kV), the incident angle is  $\sim$ 22°. In describing the orientation of HD-LR1 crystals, however, we refer to the plane of display with x and y as indicated in Fig. 5, and z coming out at  $90^{\circ}$  towards the reader. Orientation  $\perp c$  has the crystallographic c axis parallel to z and x perpendicular to  $\{11\bar{2}0\}$ , whereas orientation ||c| has c in the x-y plane albeit at a  $\sim 10^{\circ}$  angle from x due to uncertainties in the mounting. Orientations c60 and c60' (c60 rotated by  $90^{\circ}$ ) have the c axis plunging at  $\sim$ 60° from z with a slight rotation towards and away from the incoming beam direction, respectively.

Six analyses per oriented HD-LR1 piece were acquired along with analyses of NIST SRM 610 located in close spatial proximity that were used to normalize for minor instrumental drift or

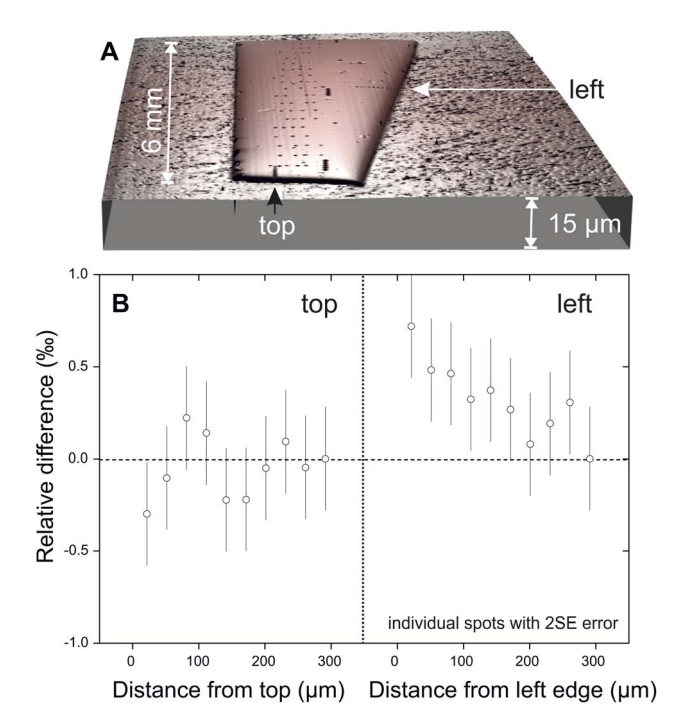


Fig. 4 Vertically exaggerated sample topography with locations of top and left edge profiles indicated by arrows (A) and relative deviation in relation to distance from the edge (most interior value set as 0) (B). 2 SE errors plotted as in Fig. 2.

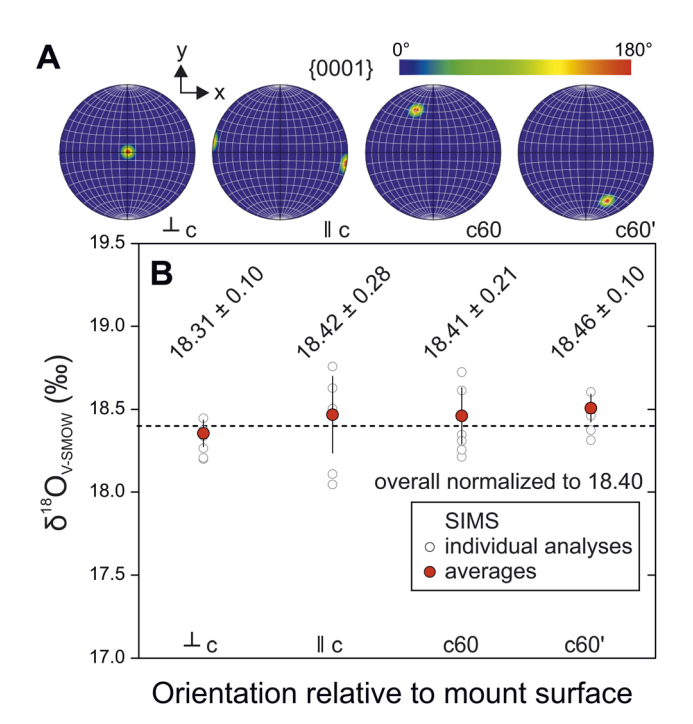


Fig. 5 EBSD pole figure of four selectively oriented pieces of HD-LR1 (A) and  $\delta^{18}$ O values for four different orientations; error bars: 2SE, plotted as in Fig. 2.; uncertainty: 1 SD (B).

possible geometry related variability due to the relatively large area over which the oriented pieces were mounted. After normalizing all data to the bulk value of 18.40% (Table 2),

a one-way ANOVA statistical test was applied and no significant dependence of the oxygen isotopic composition on crystal orientation was observed (p=0.57). Therefore, within analytical uncertainty, no crystal-geometry related bias was found for the orientations tested.

Sample topography has been documented as detrimental for achieving accurate SIMS stable isotope results, and isotopically homogeneous materials which protrude from the surrounding epoxy by several 10 s of µm can be affected by isotopic bias of several per mille when analysed at the margins.23 Achieving flat surfaces for corundum is difficult because of the extreme hardness difference relative to the epoxy used for embedding and the long polishing durations required. Surface profiles show that HD-LR1 pieces emerge from the surrounding epoxy by  $\sim 2 \mu m$  and that their surfaces are slightly convex (Fig. 4). Nonetheless, profiles in the centre of HD-LR1 show the same reproducibility as NIST SRM 610 glass, suggesting that the slight convexity is acceptable, i.e., good reproducibility is still achieved under these conditions. Approaching the edges of the corundum piece to within <100 µm, however, causes deviations by up to 0.8%, which we attribute to topography induced bias.

#### Discussion: suitability of HD-LR1 as a reference material

Accurate oxygen isotope analysis by SIMS requires matrix-matched reference materials which are ideally of the same chemical composition as the unknowns. EPMA data of HD-LR1 indicate stoichiometric  $Al_2O_3$  with only Cr as a trace component (276  $\pm$  29  $\mu g$  g $^{-1}$ ). Natural corundum has typically more impurities, but with rare exceptions, these are generally <0.6 wt% for TiO $_2$ , <1 wt% for Cr $_2O_3$ , and <1.8 wt% for Fe $_2O_3$ . We cannot rule out that minor compositional differences between HD-LR1 and natural corundum could cause slight bias in IMF but given low concentrations and considering the overall reproducibility level of SIMS analysis, these are likely negligible.

While precise (at the <0.5% 2SD level) oxygen isotope analysis by SIMS is routine for many materials, crystal orientation bias is a known issue for some minerals, including hematite that is isostructural with corundum. Variability of  $\pm 3\%$  in  $\delta^{18}$ O values was reported for SHRIMP-SI analyses of an isotopically homogeneous hematite reference material in different crystallographic orientations.15 Crystal orientation effects can be a result of channelling whereby a larger fraction of primary ions becomes implanted deeper into the lattice compared to other orientations.25 In these cases, momentum transfer to the near-surface layers and removal of secondary ions becomes less efficient resulting in a decrease in sputtering rate and a corresponding increase in  $C_s$  concentration at the projected depth. In addition, fractionation due to focusing of secondary ions has been cited when atoms are dislodged during collisions and transferred in an anisotropic medium towards the sample surface.15

Because  $\delta^{18}$ O SIMS values of HD-LR1 are largely independent of minor variations in sputter yield, primary ion channelling in corundum as a mechanism for inducing crystal orientation bias is insignificant. The observation that corundum, in contrast to hematite, lacks strong crystal orientation effects hints at a role of Fe<sup>3+</sup> with its larger ionic radius relative to Al<sup>3+</sup> and a resulting

Published on 07 December 2023. Downloaded by University of Oregon on 5/9/2024 10:19:42 PM.

Paper

larger unit cell dimension.14 A potential analogy is the presence of Fe in magnetite which displays significant crystal orientation bias compared to isostructural spinel (MgAl2O4) which lacks these effects.26 Regardless of the still unresolved causes for crystal orientation effects in certain minerals, the absence of any significant crystal orientation bias in HD-LR1 encourages the use of SIMS as a reliable method for oxygen isotope analysis of corundum at high spatial resolution.

Another concern to be addressed is the flatness of the sample mounts. This is known to be important for achieving high reproducibility of oxygen isotope analyses by SIMS, especially for materials that show strong contrasts in hardness.<sup>23</sup> Because corundum is among the hardest minerals in nature (Mohs hardness 9), it is very difficult to polish to a flat surface. Topography effects in  $\delta^{18}O$  SIMS were documented when placing spots closely (within <100 µm) onto the boundary between HD-LR1 and epoxy. We could mitigate topography effects to be mainly detectable only in the x-direction and to <0.8% even when within only 20 µm if the edge by following the preparation steps summarized in the Experimental section.

Lastly, we document that the isotopic composition of HD-LR1 shows a significant negative anomaly in  $\Delta^{\prime 17}$ O that differs from natural corundum. This  $\Delta'^{17}O$  anomaly is presumably inherited from the exchange between the precursor materials for the Al<sub>2</sub>O<sub>3</sub> melt and tropospheric O<sub>2</sub>.9 Non-zero  $\Delta'^{17}$ O values are thus a clear, but not exclusive characteristic of synthetic corundum. Moreover, meteoritic corundum can display  $\Delta'^{17}$ O anomalies, 27 and for these applications HD-LR1 with a small but significant  $\Delta'^{17}O$ depletion would also serve as a relevant secondary reference material to detect minor isotopic variations in the range of near-zero  $\Delta^{\prime 17}$ O values for meteoritic materials.

## Conclusions

We present HD-LR1 as a new matrix-matched reference material for SIMS analysis of oxygen isotopes in corundum. Originating as a synthetic laser ruby crystal, HD-LR1 is chemically homogeneous and pure, with only Cr as a trace component detected at 276  $\mu g$  g<sup>-1</sup>. The LF-IRMS average for multiple analyses of mgsized fragments yield values for  $\delta^{18}O = +18.40 \pm 0.14\%$  and  $\Delta^{\prime 17} O = -0.368 \pm 0.005\%$  (95% conf.). High spatial resolution SIMS oxygen isotope analyses confirm oxygen isotopic homogeneity at the ng-scale. Crystal orientation related bias for oxygen isotopes is insignificant, but sample topography needs to be minimized to not cause bias at the edges of grains. Because of a slight but significant negative anomaly in  $\Delta^{\prime 17}$ O compared to terrestrial corundum, HD-LR1 is ideally suited for calibration of  $\Delta'^{17}O$  in SIMS analysis, with potential applicability to cosmochemistry or natural gemstone identification. Because of the extremely low abundances of trace elements (except for Cr), HD-LR1 can serve as a matrix-matched blank for corundum in laser ablation inductively coupled mass spectrometry (LA-ICP-MS) or SIMS trace element analyses. The new matrix-matched corundum reference material HD-LR1 is available for all interested laboratories upon request.

Sebastian Schmidt: conceptualization, formal analysis, investigation, writing - original draft, writing - review & editing, visualization, project administration, funding acquisition. Andreas Hertwig: formal analysis, investigation, writing - original draft, writing - review & editing, supervision. Axel Karl Schmitt: formal analysis, investigation, writing - original draft, writing - review & editing, supervision, project administration. Katharina Cionoiu: formal analysis, investigation, writing review & editing. Kevin McKeegan: resources, writing - review & editing. Ilya Bindeman: formal analysis, investigation, writing review & editing. Tomasso Di Rocco: formal analysis, investigation, writing - review & editing. Andreas Pack: formal analvsis, investigation, writing - review & editing.

# Conflicts of interest

There are no conflicts to declare.

# Acknowledgements

We thank Ilona Fin and Oliver Wienand for skilful support in sample preparation. Sebastian Cionoiu and Hans-Peter Meyer are acknowledged for help with EBSD and electron microprobe analysis, respectively. Support through the Dr Eduard Gübelin Research Scholarship and Association, as well as valuable input by Peter Tollan and Daniel Nyfeler (Gübelin Gem Lab) is gratefully acknowledged. We also thank Aaron Palke (Gemological Institute of America, GIA) for providing the GIA corundum standards set.

## Notes and references

- 1 Q. R. Shollenberger, L. E. Borg, J. Render, S. Ebert, A. Bischoff, S. S. Russell and G. A. Brennecka, Geochim. Cosmochim. Acta, 2018, 228, 62-80.
- 2 R. B. Turnier, Y. Katzir, K. Kitajima, I. J. Orland, M. J. Spicuzza and J. W. Valley, J. Metamorph. Geol., 2019, **38**, 53-70.
- 3 E. V. Dubinsky, J. Stone-Sundberg and J. L. Emmett, Gems Gemol., 2020, 56, 2-28.
- 4 G. Giuliani and L. A. Groat, Gems Gemol., 2019, 55, 464-489.
- 5 J. Stone-Sundberg, T. Thomas, Z. Sun, Y. Guan, Z. Cole, R. Equall and J. L. Emmett, Gems Gemol., 2017, 53, 438-451.
- 6 L. A. Groat, G. Giuliani, J. Stone-Sundberg, Z. Sun, N. D. Renfro and A. C. Palke, Gems Gemol., 2019, 55, 512-535.
- 7 A. C. Palke, S. Saeseaw, N. D. Renfro, Z. Sun and S. F. McClure, Gems Gemol., 2019, 55, 580-612.
- 8 J. Wong and C. Verdel, Int. Geol. Rev., 2017, 60, 188-195.
- 9 A. Pack, Rev. Mineral. Geochem., 2021, 86, 217-240.
- 10 G. Giuliani, M. Chaussidon, H. Schubnel, D. H. Piat, C. Rollion-Bard, C. France-Lanord, D. Giard, D. Narvaez and B. Rondeau, Science, 2000, 287, 631-633.
- 11 J. M. Eiler, C. Graham and J. W. Valley, Chem. Geol., 1997, 138, 221-244.

- 12 J. Mariga, E. Ripley, C. Li, K. McKeegan, A. Schmidt and M. Groove, *Earth Planet. Sci. Lett.*, 2006, **248**, 263–275.
- 13 K. K. Wang, I. T. Graham, L. Martin, P. Voudouris, G. Giuliani, A. Lay, S. J. Harris and A. Fallick, *Minerals*, 2019, 9, 91.
- 14 L. Pauling and S. B. Hendricks, *J. Am. Chem. Soc.*, 1925, 47, 781–790.
- 15 L. White, P. Vasconcelos, J. Ávila, T. Ubide and T. Ireland, *Chem. Geol.*, 2021, 583, 120461.
- 16 *ISO Guide* 35, International Organization for Standardization, 2017.
- 17 K. Nassau, The chemistry of laser crystals, in *Applied Solid State Science*, ed. Raymond Wolfe, Elsevier, 1971, vol. 2, pp. 173–299.
- 18 P. Baertschi, Earth Planet. Sci. Lett., 1976, 31, 341-344.
- 19 I. N. Bindeman, D. A. Ionov, P. M. E. Tollan and A. V. Golovin, *Nat. Commun.*, 2022, 13, 3779.
- 20 J. W. Valley, N. Kitchen, M. J. Kohn, C. R. Niendorf and M. J. Spicuzza, *Geochim. Cosmochim. Acta*, 1995, 59, 5223– 5231.

- 21 M. F. Miller, A. Pack, I. N. Bindeman and R. C. Greenwood, Chem. Geol., 2020, 532, 119332.
- 22 A. Pack, R. Tanaka, M. Hering, S. Sengupta, S. Peters and E. Nakamura, *Rapid Commun. Mass Spectrom.*, 2016, 30, 1495–1504.
- 23 N. T. Kita, T. Ushikubo, B. Fu and J. W. Valley, *Chem. Geol.*, 2009, 264, 43–57.
- 24 W. A. Deer, R. A. Howie and J. Zussman, *5A: Non-silicates:* oxides, hydroxides and sulphides, Geological Society, London, 2011.
- 25 A. Benninghoven, F. G. Rudenauer and H. W. Werner, Secondary ion mass spectrometry: basic concepts, John Wiley & Sons, New York, 1987.
- 26 J. M. Huberty, N. T. Kita, R. Kozdon, P. R. Heck, J. H. Fournelle, M. J. Spicuzza, H. Xu and J. W. Valley, *Chem. Geol.*, 2010, 276, 269–283.
- 27 A. N. Krot, C. Ma, K. Nagashima, A. M. Davis, J. R. Beckett, S. B. Simon, M. Komatsu, T. J. Fagan, F. Brenker, M. A. Ivanova and A. Bischoff, *Geochemistry*, 2019, 79, 125519.